NJC

Accepted Manuscript

This is an *Accepted Manuscript*, which has been through the Royal Society of Chemistry peer review process and has been accepted for publication.

Accepted Manuscripts are published online shortly after acceptance, before technical editing, formatting and proof reading. Using this free service, authors can make their results available to the community, in citable form, before we publish the edited article. We will replace this *Accepted Manuscript* with the edited and formatted *Advance Article* as soon as it is available.

You can find more information about *Accepted Manuscripts* in the Information for Authors.

Please note that technical editing may introduce minor changes to the text and/or graphics, which may alter content. The journal's standard Terms & Conditions and the Ethical guidelines still apply. In no event shall the Royal Society of Chemistry be held responsible for any errors or omissions in this *Accepted Manuscript* or any consequences arising from the use of any information it contains.

ROYAL SOCIETY OF CHEMISTRY

www.rsc.org/njc

A stable superhydrophobic surface with excellent anti-corrosion, anti-icing and deicing properties has been fabricated via annealing treatment from superhydrophilic surface.

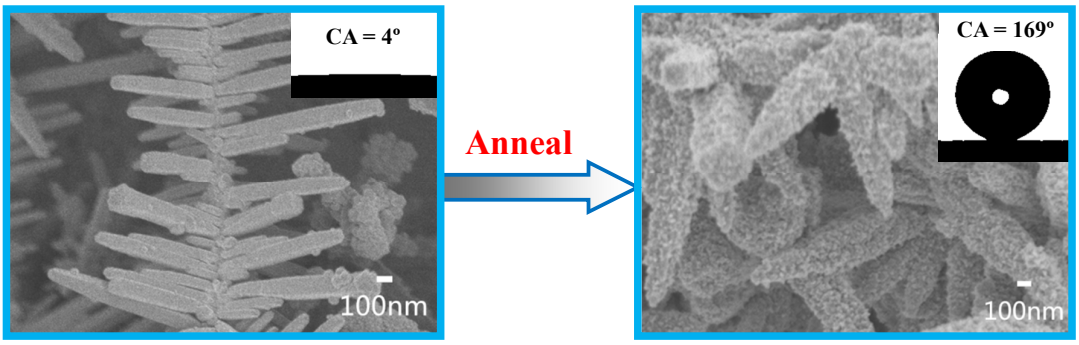

Cite this: DOI: 10.1039/c0xx00000x

www.rsc.org/xxxxxx

ARTICLE TYPE

Controllable wettability of micro- and nano- dendritic structures formed on aluminum substrates

Yuanyuan Cheng, Shixiang Lu* and Wenguo Xu*

Received (in XXX, XXX) Xth XXXXXXXXX 20XX, Accepted Xth XXXXXXXXX 20XX
DOI: 10.1039/b000000x

Superhydrophilic surface with a static water contact angle of 4±2 °via two-step immersion process and superhydrophobic surface with a static water contact angle of 169±2 °and a sliding angle of almost 0 ° via succedent thermal treatment have been successfully fabricated on aluminum substrates. The surface morphologies and chemical compositions were investigated using field emission scanning electron microscopy, x-ray powder diffraction and x-ray photoelectron spectroscopy, and the formation mechanism was also analyzed. The thermal treatment which causes the generation of oxides and the appearance of nano-sized particles is very important for the surface characteristic transformation from superhydrophilicity to superhydrophobicity. The effects of various experimental parameters on wettability, corrosion resistance, anti-icing and deicing properties, stability and large-area preparation were also studied. The corrosion rate of the as-prepared superhydrophobic surface decreases by about 57.6 times compared with that of the untreated aluminum surface and appropriately 34.8 times compared with that of the pure copper surface. These excellent properties of the superhydrophobic surface may be favorable for its potential applications and industrialization.

Introduction

The wettability of solid surfaces has significant values for the fundamental research and practical applications. In the year 1997, superhydrophobic surfaces with CA larger than 150 ° and superhydrophilic surfaces with considerably small CA were reported separately by Barthlott and Neinhuis[1] and Fujishima's[2] group. Since then, the superhydrophobic and superhydrophilic surfaces have been paid close attention owing to their very special wettability and important applications.[3-6] Superhydrophobic surface is defined as a surface with a static water contact angle (CA) larger than 150 °and a sliding angle (SA) lower than 10 °. Superhydrophilic surface refers to the surface with a static water CA lower than 5 °. The wettability of solid surfaces can be controlled by surface topography and/or surface chemistry. With this controllability, many useful methods have been introduced to produce superhydrophobic and superhydrophilic surfaces. Such as, template method,[7,8] electro-spinning,[9-11] sol-gel method,[12-14] layer-by-layer technique,[15-17] etching treatment,[18-20] chemical vapor deposition (CVD),[21-23] electroless galvanic deposition[24-26] and electrochemical deposition.[27-31]

Among these, the electroless galvanic deposition method that involves galvanic reactions has been used to fabricate superhydrophobic surfaces for many years.[32-34] The deposition can occur spontaneously when metallic ions are in contact with a metal substrate of lower oxidation potential. Thus, electroless deposition is a low-cost and efficient method to roughen metal substrates. Zang *et al.* developed a straightforward method to tune the wettability of an aluminum substrate by chemical deposition method and fluoroalkylsilane (FAS) modification and a bouncing behavior has also been observed for droplets impinging on the superhydrophobic substrate, suggesting its potential application as a self-cleaning surface.[34] Tian *et al.* studied the wetting property of porous copper nanowall arrays prepared by a facile replacement reaction, and found that the flower-like hierarchical structures can be formed on zinc substrates and the surfaces showed good hydrophobicity.[35] Qi *et al.* discovered that silver nanoparticles can be successfully coated on the surface of stainless steel needle by a simple electroless replacement reaction process, and after modified with thiol molecules, the surfaces exhibited excellent superhydrophobicity and antibacterial property.[36] Liu *et al.* fabricated superhydrophobic surfaces by means of heterogeneous nucleation and growth of lotus-leaf-like boehmite on aluminum foil, and the surfaces exhibited non-sticking behavior, long-term storage stability and relatively good mechanical strength.[37] Nevertheless, most of them used organic substances as the modification, which may be environmentally unfriendly and toxic, and required specialized equipment and/or complicated processing (temperature, time and chemicals), which limits widespread utilization of the methods for large-scale production. Therefore, it could be desirable to design an efficient, nontoxic and low-cost method for fabricating superhydrophobic surfaces which can be used in large-scale production.

We have been attracted to fabricate wettability surfaces on various metal substrates without any organic modification for many years.[24-26] In this paper, the fabrication of superhydrophobic surface is presented with a static water contact angle of 169±2 °and a sliding

angle of approximately 0 º via two-step immersion processes and succedent thermal treatment on aluminum substrates. If the thermal treatment isn't used, the surface is superhydrophilic with a static water contact angle of 4±2 º. The generation of oxides and the appearance of nano-sized particles are important for the surface characteristic transformation from superhydrophilicity to superhydrophobicity. The corrosion resistance of the as-prepared superhydrophobic surface, untreated aluminum surface and pure copper surface has been obtained by the potentiodynamic polarization curves (Tafel) and the superhydrophobic surface is the most excellent and important for the application in more fields. The anti-icing and deicing properties of the superhydrophobic surface and untreated aluminum surface are tested respectively, and of course, the superhydrophobic surface exhibits excellent anti-icing and deicing properties and this may be useful for constructing multifunctional outdoor devices. The large-area superhydrophobic surface is also produced and may be helpful for industrialization.

Experimental

Materials

Copper dichloride dihydrate ($CuCl_2 \cdot 2H_2O$, 99.0%), sodium hydroxide (NaOH, 96.0%), ethanol (CH_3CH_2OH, 99.7%) and sodium chloride (NaCl, 99.5%) were analytic grade reagents without further purification and were purchased from Sinopharm Chemical Reagent Co., Ltd. Aluminum substrates (99.9%) were obtained from Beijing Nonferrous Metal Research Institute.

Preparation of samples

Aluminum substrates with size of 1.0cm × 1.0cm × 0.1cm were successively washed in an ultrasonic bath with ethanol and deionized water for 10 min respectively to remove surface grease. Subsequently, they were set vertically in an unplasticized poly vinyl chloride (UPVC) tube without a bottom as shown in our previous report,[24,26] and then were immersed in 0.01 mol/L NaOH alkaline solution for 4 min. After that, in the same way, the etched samples were placed in 0.02 mol/L $CuCl_2$ aqueous solution for 20 min in air atmosphere. After the two-step immersion processes, the samples were annealed in an oven at 150℃ for 2 h in open air. All the treated substrates were rinsed thoroughly with deionized water and dried in the air for several minutes prior to the next step.

Samples characterization

The surface morphologies were characterized using a field emission scanning electron microscope (FESEM, JSM-7500F, JEOL, Japan) and the operating voltage was 2.0 kV. The crystal structure was determined by x-ray powder diffractometer (XRD, D8 Advance, Bruker, Germany) with Cu Kα radiation at a continuous scanning mode (40 kV, 40 mA, and λ = 0.15418 nm) and scanning rate of 3 º/min. X-ray photoelectron spectrometer (XPS, PHI Quantera II, Ulvac-Phi, Japan) was employed to characterize the surface compositions of the resulting surfaces using 25 W Al Kα (1486.6 eV) x-ray as the excitation source. The static water contact angles (CAs) and sliding angles (SAs) were measured by remote computer-controlled goniometer system (FTÅ 200, Dataphysics Inc., USA) equipped with a video camera (Canon) and a tilting stage. SAs were measured by slowly tilting the sample stage until the water droplet started moving. Water droplets (8 μL) were carefully dropped onto the surfaces, and the average value of five measurements obtained at different positions was used as the final CA. All values of each sample are in a range of ± 2 º, as is error bars in figures. The electrochemical measurements were conducted in 3.5 wt % aqueous solutions of NaCl at room temperature (25℃) in open air without stirring using electrochemical workstation (CHI 760E, CH Instruments Inc., China). The electrochemical corrosion tests were carried out using a three-electrode configuration with platinum as the counter electrode, saturated calomel as the reference electrode, and the samples with an exposed area of 1 cm^2 as the working electrode. The polarization curves were obtained at a sweep rate of 2 mV/s. Tribological property was evaluated using a UMT Universal Mechanical Tester (UMT-2, Bruker, USA). The tribology experiment was operated by a load, which ranged from 2 N to 10 N using a sharp diamond drill. The moving rate of the diamond drill during the scratch process was 0.02 mm/s and the one-way scratch length was 5 mm. The relevant experimental parameters were obtained using a realtime control computer and data analysis software.

Results and discussion

Surface morphology and wettability

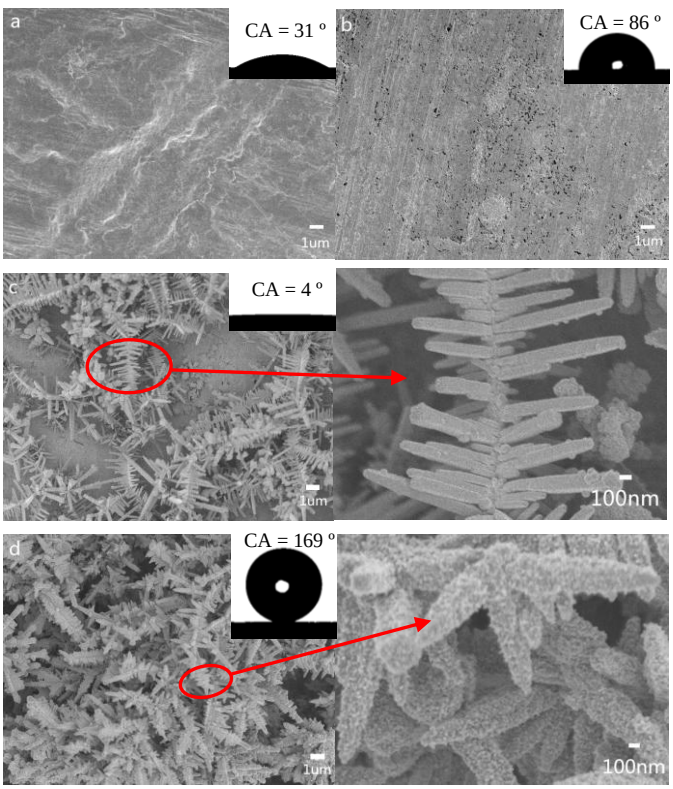

Fig. 1. FESEM images and water CAs: (a) untreated aluminum surface, (b) sample surface after etched with 0.01 mol/L NaOH solution for 4 min, (c) sample surface after immersed in 0.02 mol/L $CuCl_2$ solution for 20 min, (d) sample surface after annealed in an oven at 150℃ for 2 h. The insets are the static water CAs.

Fig. 1 shows the FESEM images and water CAs on the different surfaces, which clearly demonstrate the changes on wettability of aluminum surfaces. The untreated aluminum surface is smooth with a static water CA of 31±2 º, indicating

hydrophilicity as shown in Fig. 1a. A large number of holes, after etched with NaOH solution, are irregularly distributed on the surface and some of them link together to form a larger one. This surface is still hydrophilic with a water CA of 86±2 º as shown in Fig. 1b. After subsequent immersion with $CuCl_2$ solution, there are a lot of dendritic structures in all directions, which consist of elemental Cu from electroless galvanic deposition that can be observed in the XRD pattern (Fig. 2c). The magnified FESEM image of an individual dendrite shows the Cu dendrite is composed of a pronounced trunk and numerous leaves. Although there are dendritic structures on the surface, the water CA dramatically decreases to 4±2 º and the water droplets completely spread on the superhydrophilic surfaces via the two-step immersion processes as shown in Fig. 1c. Then the surface was annealed in an oven at 150 ℃ for 2 h, and the dendritic structures became stronger and tighter. Moreover, the nano-sized particles emerged on the leaves and this may be due to the generation of CuO via the thermal treatment, which can be observed from the XRD and XPS spectra in Fig. 2d and Fig. 3. The character of the surface dramatically changes from superhydrophilicity to superhydrophobicity, with a static water CA of 169±2 º and a water sliding angle of approximately 0 º as shown in Fig. 1d and Video S1. Obviously, the thermal treatment which causes the generation of oxides (decreasing the surface free energy) and the appearance of nano-sized particles (fabricating micro- and nano- hierarchical structures) is very important for the superhydrophobicity.

Surface composition

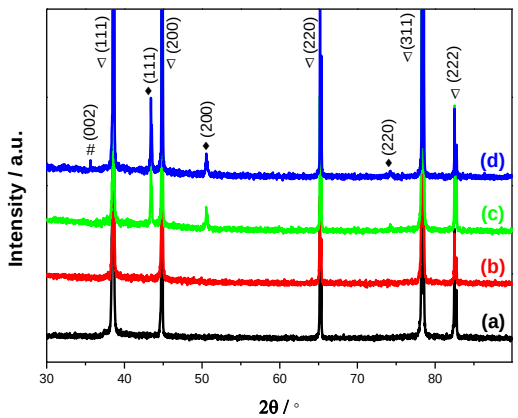

Fig. 2. XRD spectra: (a) untreated aluminum surface, (b) sample surface after etched with 0.01 mol/L NaOH solution for 4 min, (c) sample surface after immersed in 0.02 mol/L $CuCl_2$ solution for 20 min, (d) sample surface after annealed in an oven at 150 ℃ for 2 h. The symbols of ▽, ◆ and # represent the peaks of Al, Cu and CuO respectively.

Fig. 2 shows the XRD spectra of the untreated, etched with NaOH solution, immersed in $CuCl_2$ solution and the resulting superhydrophobic surfaces. The symbols of ▽and ◆represent the peaks of Al and Cu respectively. As a comparison, the XRD pattern of the bare Al is attributed to the untreated aluminum surface as shown in Fig. 2a. The sharp peaks at 2θ = 38.61 º, 44.89 º, 65.23 º, 78.31 º and 82.54 º are assigned to the diffraction peaks of Al(111), Al(200), Al(220), Al(311), and Al(222) respectively (JCPDS Card No. 04-0787). After etching process, positions of the peaks keep unchanged, and no new substances are generated as shown in Fig. 2b. After subsequent immersion process, Cu deposit on the aluminum surface, and three new peaks appear in the region of 30 º-90 º. The peaks at 2θ = 43.46 º, 50.64 º and 74.25 º are assigned to the characteristic peaks of Cu(111), Cu(200) and Cu(220) planes of the face-centered cubic Cu crystals (JCPDS card No. 04-0836) as shown in Fig. 2c. The intensity of Cu(111) plane is evidently stronger than that of other planes, indicating a preferential growth of Cu crystals along the (111) plane. After thermal treatment, the peak at 2θ = 35.59 º is assigned to the diffraction peak of CuO(002) as shown in Fig. 2d, indicating the generation of CuO (JCPDS Card No. 45-0937). However, no peaks are assigned to crystalline aluminum oxide, which is indicative of the small size and/or very well-dispersed crystallites below the detection limit for XRD, or existence of amorphous phase.[38,39]

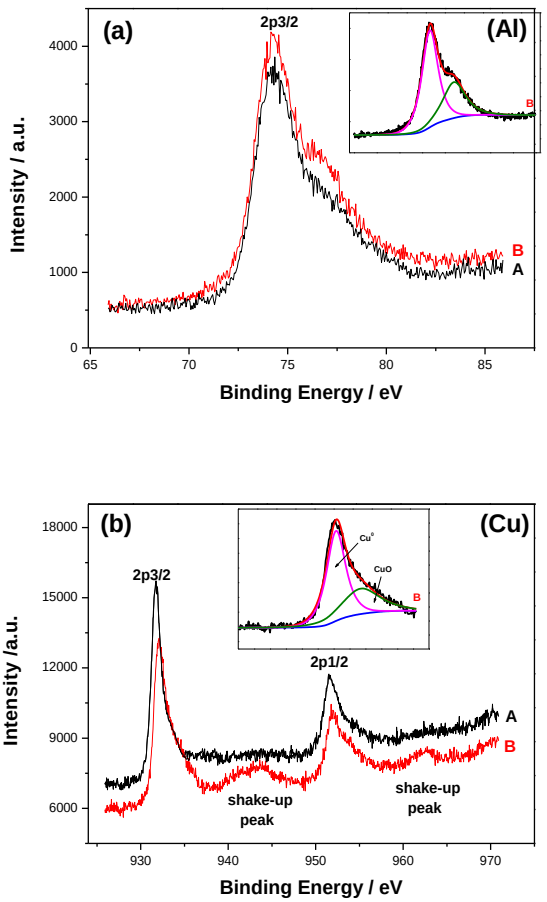

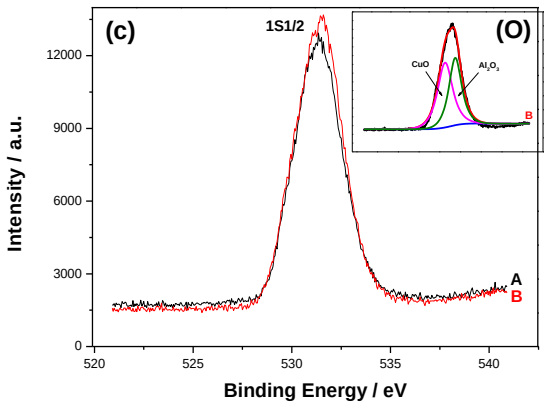

Fig. 3. XPS spectra: (a) Al region, (b) Cu region, (c) O region; (A) before annealing, (B) after annealing. The insets are fitting curves of the corresponding lines.

In order to further demonstrate the effect of the thermal treatment on the surface characteristic transformation from superhydrophilicity to superhydrophobicity, and to obtain detailed information on the chemical states of ions, XPS was performed as shown in Fig. 3. In the Al region as shown in Fig. 3a, a peak with a binding energy of 74.3 eV is associated to Al 2p3/2 emission,[40,41] and this means Al always exists on the surfaces whether annealed or not and this also can be demonstrated by the XRD spectra in Fig. 2. After annealing treatment, the shoulder peak at the higher binding energy of fitting curve B appears and this may be due to the generation of Al_2O_3.[42,43]

In the Cu region as shown in Fig. 3b, Cu 2p3/2 and Cu 2p1/2 core level peaks (here only Cu 2p3/2 is discussed, because Cu 2p3/2 and Cu 2p1/2 play similar roles in determining the Cu valence) are measured to determine copper valences. The presence of the $\pi - \pi^*$ shake-up peaks and O 1s peaks are characteristic of Cu^{2+} and O^{2-} species[44], suggesting that CuO presents on the surface after annealing treatment and this also can be verified by the XRD pattern (Fig. 2d). As is reported,[45-47] the peak at 933.6 eV is assigned to CuO and the peak at 932.2 eV is related to low valence copper species. The Cu^0 species are proved to present on the surfaces from the XRD pattern (Fig. 2c and d). Some elemental Cu is oxidized to CuO after annealing treatment.

The O 1s1/2 peak of the fitting curve B as shown in Fig. 3c, can be resolved into two overlapping components; the peak at 530.7 eV is attributed to the O^{2-} of CuO species and the peak at 531.9 eV is ascribed to the O^{2-} of Al_2O_3 species. The existence of Al_2O_3 and CuO is one of the reasons for the superhydrophobicity.

Analysis of mechanism

Combining with the analyses of FESEM, XRD and XPS above, the formation mechanism of the superhydrophilic and superhydrophobic surfaces can be concluded as shown in Scheme 1. While the aluminum substrates were firstly immersed into the 0.01 mol/L NaOH aqueous solution for 4 min, the surfaces were damaged instantaneously and some holes appeared. Then the surfaces were immersed into 0.02 mol/L $CuCl_2$ aqueous solution for 20 min, and Cu^{2+} ions reacted with the surfaces via electroless galvanic deposition which resulted in the deposition of Cu. After the two-step immersion processes, the surface exhibited superhydrophilicity with a static water contact angle of 4±2 º. Owing to the standard electrode potentials of Al/Al^{3+} and Cu^{2-}/Cu are 1.662 V and 0.340 V respectively, the chemical substitution reaction can occur spontaneously in the air. Finally, when the substrates were annealed in an oven at 150℃ for 2 h, Cu and Al were oxidized to CuO and Al_2O_3 respectively and the surface characteristic turned to superhydrophobicity with a static water contact angle of 169±2 º. All the reactions involved are listed as follows.

$$2Al + 2OH^- + 6H_2O \rightarrow 2[Al(OH)_4]^- + 3H_2\uparrow \quad (1)$$

$$2Al + 3Cu^{2+} \rightarrow 2Al^{3+} + 3Cu \quad (2)$$

$$2Cu + O_2 \rightarrow 2CuO \quad (3)$$

$$4Al + 3O_2 \rightarrow 2Al_2O_3 \quad (4)$$

Scheme 1. The main reactions in the formation of superhydrophilic and superhydrophobic surfaces.

Theoretical explanation for wettability

The resulting superhydrophobic surface has a static water contact angle of 169±2 ºand a sliding angle of almost 0 º, and this may be due to the appearance of nano-sized particles and the generation of oxides (CuO and Al_2O_3). To further demonstrate the superhydrophobicity of this composite surface, we study the wetting behavior on CuO (smooth copper substrate after annealing treatment), Al_2O_3 (smooth aluminum substrate after annealing treatment) and superhydrophobic surfaces respectively. The water contact angles on these surfaces are 81±2 º, 69±2 ºand 169±2 ºrespectively as shown in Fig. 4.

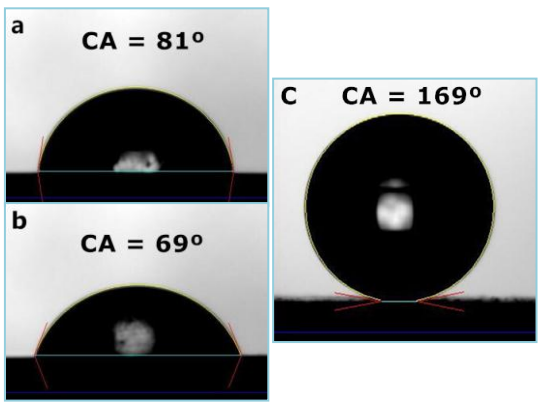

Fig. 4. The water CAs on CuO (a), Al_2O_3 (b) and superhydrophobic (c) surfaces respectively.

Wenzel[48] and Cassie[49] have each offered a theory for the surface wettability. Wenzel's model describes the wetting of a surface which has been totally wetted by liquid, and there are no gas bubbles between the liquid and solid surface. On the other hand, Cassie's model describes the wettability of a surface on which gas bubbles reside between the liquid and solid, and the surface is not completely wet.

For the sample surface before annealing treatment, it is completely superhydrophilicity with a water CA of 4 ºand the water droplet is

totally sticky to the surface, so the Wenzel model[50] is applicable. According to the Wenzel's equation,

$$\text{Cos } \theta^* = r \text{ Cos } \theta \quad (5)$$

where θ^* is the apparent contact angle on a rough surface, θ is the equilibrium contact angle on a smooth surface, and r is the surface roughness defined as specific area ratio between the real and projected solid-liquid contact area. Here, given that $\theta^* = 4°$ (rough surface before annealing treatment) and $\theta = 31°$ (smooth substrate before annealing treatment), and r is calculated as 1.164. That is, the value of real solid-liquid contact area is as 1.164 times as that of the projected on the superhydrophilic surface. This result accords with the assumption that hydrophilicity of hydrophilic surface as roughness increases.

For the sample surface after annealing treatment, it is completely superhydrophobicity with a water CA of 169 °and there is no sticky behaviour with a water sliding angle of approximately 0 °, the water droplet is totally sticky to the surface, so the Cassie-Baxter model[50] is considered. According to the Cassie-Baxter equation,

$$\text{Cos } \theta^* = f_1 \text{ Cos } \theta - f_2 \quad (6)$$

Where θ^* and θ represent the apparent contact angle on a rough surface and the equilibrium contact angle on a smooth surface respectively; f_1 and f_2 are the area fractions of the solid and air on the surface respectively and $f_1 + f_2 = 1$. Given that $\theta^* = 169°$ (rough surface after annealing treatment) and $\theta = 69°$ (smooth substrate after annealing treatment), f_1 and f_2 are estimated as 0.0135 and 0.9865 respectively. These data indicate that when a water droplet is placed on a superhydrophobic surface, approximately 1.35 % serves as the contact area of the water droplet and the solid surface, and the remaining 98.65 % serves as the contact area of the water droplet and air. This demonstrates that a liquid droplet sits on asperities generating air cavities and giving rise to decrease in solid-liquid interface and increase in liquid-vapour interface.

In general, the surface free energies of solid substances are far more than that of organic substances.[51,52] So, organic substances were usually used for modifying the roughness surfaces to obtain superhydrophobicity. For example, Shi[53] *et al.* presented that nano-silica particles were deposited on acid-etched aluminum substrates to obtain a rough two-length-scale hierarchical structure, and then after coupled with low surface energy of fluorosilane, the surface showed superhydrophobicity. However, others' reports demonstrated that metal oxide sometimes can show superhydrophobicity without any organic modification. Such as, Huang[54] *et al.* reported a stable superhydrophobic surface via aligned carbon nanotubes (CNTs) coated with a zinc oxide (ZnO) thin film; Feng[55] *et al.* fabricated controllable wettability of aligned Zn on nano-rod films which showed superhydrophobicity under suitable conditions. In our study, the annealing treatment was used instead of organic modification to obtain superhydrophobic surface with micro- and nano- hierarchical structures.

Effects of various experimental parameters on wettability

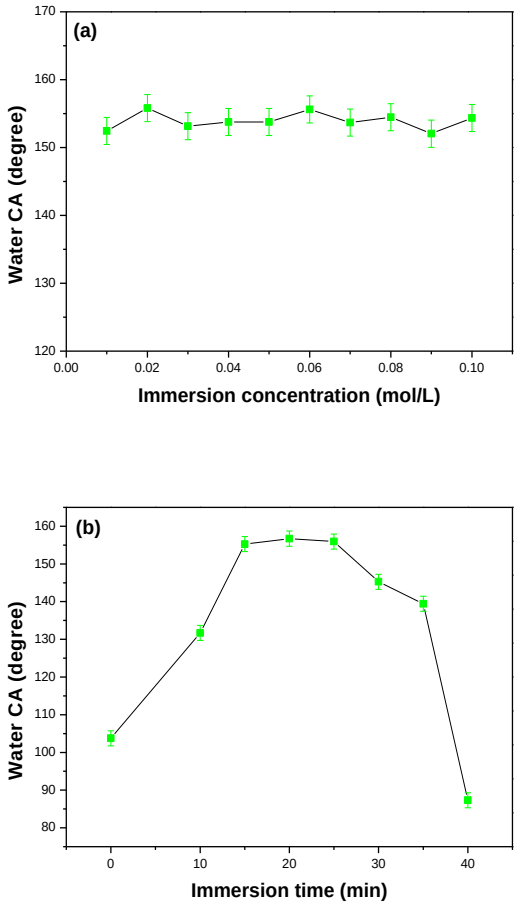

Fig. 5. Variation in the static water CAs of the surfaces with the immersion concentration (a) and immersion time (b).

We have studied the effects of the immersion time and concentration on wettability respectively and found that the appropriate immersion time is pivotal, and the concentration is not so rigorous which will benefit the fabrication of large-area surface. Fig. 5a and b show the variation in the static water CAs of the surfaces with the immersion concentration and time respectively. As shown in Fig 5a, the aluminum substrates were etched with 0.01 mol/L NaOH solution for 4 min, and then were immersed in $CuCl_2$ solution of 0.01, 0.02, 0.03, 0.04, 0.05, 0.06, 0.07, 0.08, 0.09 and 0.10 mol/L for 20 min respectively and annealed in an oven at 150℃ for 2 h. The best static water CA was 169±2 °, which appeared in the 0.02 mol/L $CuCl_2$ solution, and moreover, the static water CAs at other concentrations were also larger than 150 °. Thus, the influence of the concentrations of the $CuCl_2$ solution doesn't matter much and this will be beneficial for the fabrication of large-area surface and then may promote the industrialization.

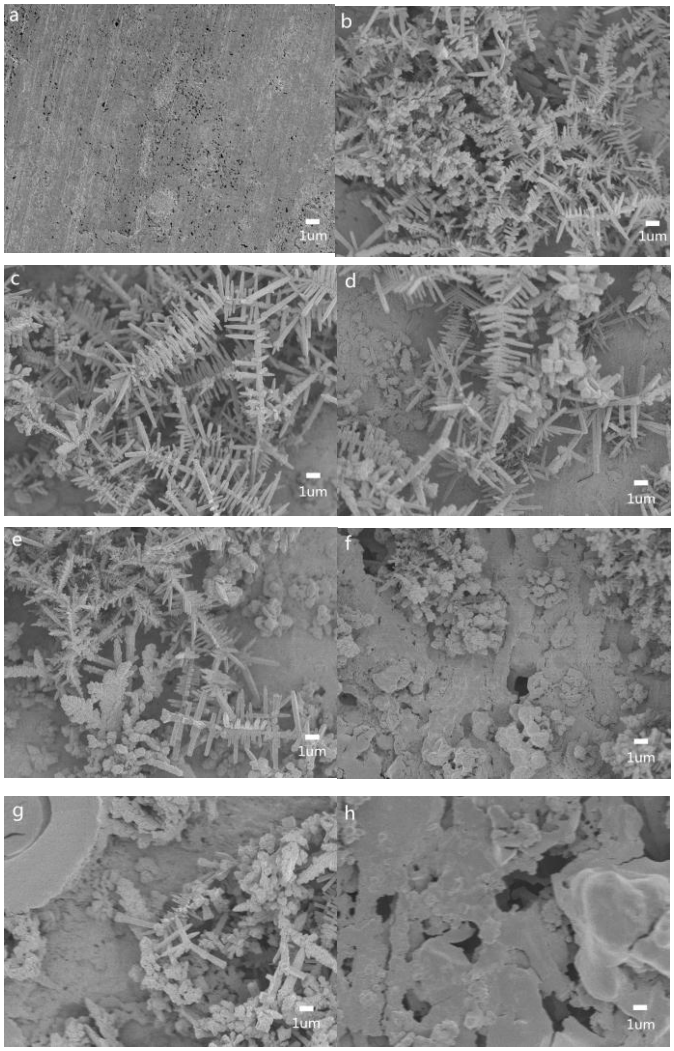

Fig. 6. The FESEM images of the surfaces with different immersion time: (a) 0, (b) 10, (c) 15, (d) 20, (e) 25, (f) 30, (g) 35, (h) 40 min.

The effect of immersion time on wettability was investigated by immersing the surfaces into 0.02 mol/L $CuCl_2$ solution for 0, 10, 15, 20, 25, 30, 35 and 40 min respectively, and other conditions unchanged as shown in Fig. 5b. The largest static water CA of 169±2 ° appeared at 20th minute which indicated superhydrophobicity. Besides, the superhydrophobicity was also exhibited from 15th to 25th minute, which meant the reaction condition was not too strict. The different surface morphologies with the varying immersion time were shown by FESEM images in Fig. 6. We can clearly see that when the immersion time was less than 10 min, the sizes of dendritic structures were less than 1 μm as shown in Fig. 6b. With the increase of immersion time, the structures grew up gradually while the sizes were always between 1 μm to 3 μm as shown in Fig. 6c-e. Soon afterwards, more and more bulk-like structures presented on the surfaces until the whole surfaces were completely covered by this new structure as shown in Fig. 6f-h. Obviously, only the suitable immersion time was conducted, can the superhydrophobic surface be fabricated.

Corrosion resistance

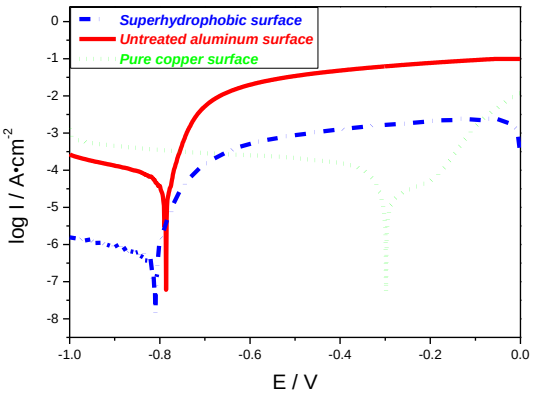

Fig. 7. Potentiodynamic polarization curves of the superhydrophobic surface (blue line), untreated aluminum surface (red line) and pure copper surface (green line) after immersed in 3.5 wt % NaCl aqueous solution.

Samples	E_{corr} (V)	i_{corr} (A/cm^2)	P_i (mm/y)
Superhydrophobic surface	−0.81	1.84 × 10^{-6}	4.20 × 10^{-5}
Untreated aluminum surface	-0.78	1.06 × 10^{-4}	2.42 × 10^{-3}
Pure copper surface	−0.30	6.38 × 10^{-5}	1.46 × 10^{-3}

Table 1. Corrosion potential (E_{corr}), corrosion current (i_{corr}) and corrosion rate (P_i) of the superhydrophobic surface, untreated aluminum surface and pure copper surface respectively.

To investigate the instantaneous corrosion rate, the potentiodynamic polarization curves (Tafel) is tested. Fig. 7 shows the potentiodynamic polarization curves of as-prepared superhydrophobic surface, untreated aluminum surface and pure copper surface respectively in 3.5 wt% NaCl solution using the Tafel extrapolation method. The results of potentiodynamic polarization test are summarized in Table 1. Corrosion potential (E_{corr}), corrosion current density (i_{corr}) and corrosion rate (P_i) are often applied to evaluate the corrosion protective property of the surfaces. The results clearly show that the E_{corr} positively increases from -0.81 V of the as-prepared superhydrophobic surface to -0.78 V of the untreated aluminum surface and then to -0.30 V of the pure copper surface. The corrosion current density and corrosion rate of the surfaces are further considered. The values of i_{corr} on the as-prepared superhydrophobic surface, the untreated aluminum surface and the pure copper surface respectively are 1.84 × 10^{-6} A/cm^2, 1.06 × 10^{-4} A/cm^2 and 6.38 × 10^{-5} A/cm^2. The i_{corr} of the superhydrophobic surface is approximately 1.74% of the untreated aluminum surface and about 2.88% of the pure copper surface, suggesting that the as-prepared superhydrophobic surface has a better corrosion resistance performance and can be used in more fields. Then the corrosion rate P_i (mm/y) of the surfaces is calculated according to following empirical equation (7).[56,57]

$$P_i = 22.85 \times i_{corr} \quad (7)$$

So the P_i of the as-prepared superhydrophobic surface (4.20 × 10^{-5} mm/y) decreases by about 57.6 times compared with that of the untreated aluminum surface (2.42 × 10^{-3} mm/y) and

appropriately 34.8 times compared with that of the pure copper surface (1.46×10^{-3} mm/y). Obviously, all these results indicate that the corrosion resistance of the superhydrophobic surface is improved drastically and is in accord with the previously published reports.[26,57]

Anti-icing and deicing properties of the superhydrophobic surface

Aluminum, as an important engineering material, has received much attention in industries owing to its easy accessibility, excellent machinability, high fatigue strength and low price.[58,59] Accordingly, they have achieved extensive industrial applications, especially in the fields of overhead cables, doors and windows, automobile wheels hub and body, etc. However, ice accretion, as a nature phenomenon, occurs easily on the metal surface under a cold condition, such as in the weather of freezing rain and wet snow. However, ice accretion will impede metal properties, damage the surface and even shorten service life. Thus, fabrication of ice-phobic surface on metal substance is imperative and necessitous. Here, ice-phobic properties of the superhydrophobic surface were also investigated. Fig. 8a shows the superhydrophobic surface and untreated aluminum surface, on which there were water droplets respectively, were placed on a glass slide under a cold condition of about -15℃ in the fridge. After about 20 min as shown in Fig. 8b, the water droplet on the untreated aluminum surface started turning to ice, but, the water droplet on the superhydrophobic surface still kept transparent liquid state. After about another 20 min as shown in Fig. 8c, the water droplet on the untreated aluminum surface had frozen completely, and yet that on the superhydrophobic surface had just a tendency to freeze. Obviously, the superhydrophobic surface effectively mitigated the freezing process and reduced ice accumulation. Thus, the superhydrophobic surfaces possess anti-icing property and this may offer more possibilities for potential outdoor application.

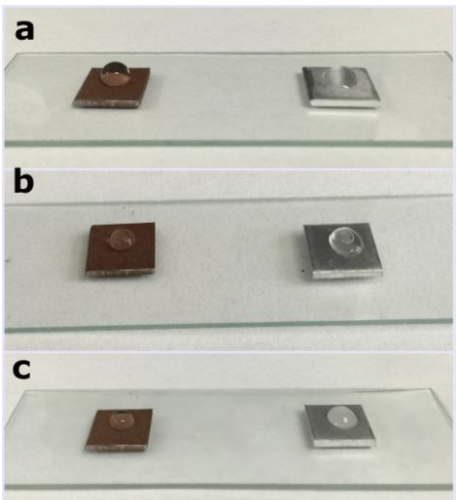

Fig. 8. Water droplets on the superhydrophobic surface (left) and untreated aluminum surface (right), respectively, after 0 (a), 20 (b), 40 (c) min under a cold condition of about -15℃ in the fridge.

As previously reported,[60,61] the anti-icing performance of superhydrophobic surface may be very limited and though ice accretion on such surfaces can be delayed, it can't be inhibited completely. Therefore, we further study the deicing property of the superhydrophobic surface. The ice, which was just taken out from fridge, was quickly placed on the superhydrophobic surface at room temperature of about 25℃ and we recorded this process with video as shown in Video S2. We can clearly see that the ice on the superhydrophobic surface thaws soon and melts into liquid droplet completely after about 90 s. Then we tilt the surface slightly, and the water droplet rolls down from the surface successfully. The superhydrophobicity is not destroyed and degraded because of deicing process. Thus, the deicing property of our superhydrophobic surface is durable and this may be valuable for more outdoor applications.

All the tests and results above indicate that the resulting superhydrophobic surface has excellent anti-icing and deicing properties, which offers possibilities to construct multifunctional outdoor devices, and may have important potential applications.

Tribological study of the superhydrophobic surface

A uniform load was used in the scratch test to analyze the bonding strength between the film and the substrate. For composite surface, the critical load appears at the point, where the coefficient of friction values abruptly increase or decrease. This critical load indicates the transition of the wear regime from one material to another material, and also means that the superhydrophobic coating is completely peeled off from the substrate surface. The variation in coefficient of friction with load for superhydrophobic surface is shown in Fig. 9. It is noticeable that the fluctuation of the friction levels before 9 N is mild. However, the applied load beyond 9 N has significant effect on coefficient of friction, and the friction coefficient decreases considerably to a low level with increasing load before seizure. The lowest levels in coefficient of friction curve clearly occurred before seizure of 10 N. We can clearly see that the critical load is about 9 N, which exhibits good binding ability. This should be attributed to the annealing treatment, which leads to the generation of oxides, and then enhances the affinity of substrate and the coating. This excellent mechanical property of the superhydrophobic surface is important for its various applications, such as anti-corrosion, anti-icing and deicing properties, and may provide more values for its potential applications.

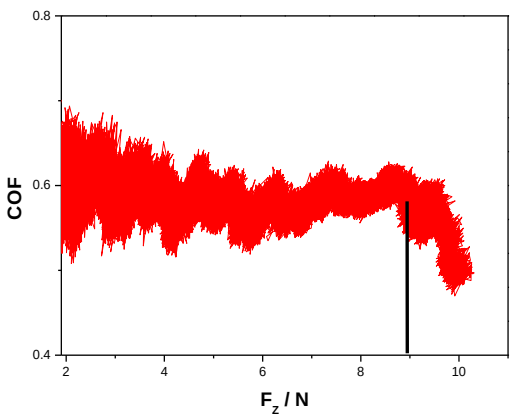

Fig. 9. The variation in coefficient of friction with load for superhydrophobic surface.

Stability and fabrication of large-area superhydrophobic surface

The superhydrophobic surface was exposed to air for 12 months to test the environmental stability and durability. The value of the static water CA was unchanged still, indicating that this novel superhydrophobic composite surface has long-term stability and durability in air atmosphere.

Fig. 10 shows a production of a large-area superhydrophobic surface. The area of this plate (10cm × 10cm) was 100 times the size of the aluminum substrate (1cm × 1cm) used in the aforementioned experiment, and the same preparing processes were used. Similarly, after thermal treatment, the surfaces were easily transformed into superhydrophobic surfaces on which the water droplets could stand. This low-cost and novel method offers possibilities to prepare large-area superhydrophobic surface and this may be beneficial for industrialization and may have important potential applications.

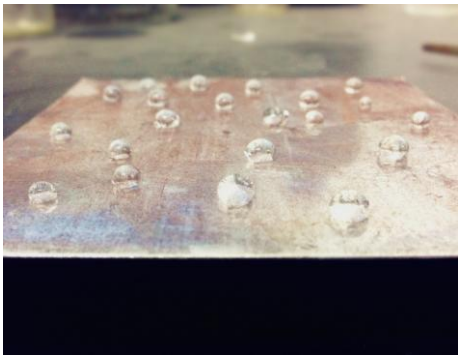

Fig. 10. The digital image of the large-area superhydrophobic surface.

Conclusions

In the present study, superhydrophilic surface with a static water contact angle of $4 \pm 2^{\circ}$ via two-step immersion processes and superhydrophobic surface with a static water contact angle of $169 \pm 2^{\circ}$ and a sliding angle of approximately 0° via succedent thermal treatment have been successfully fabricated on aluminum substrates. The various experimental parameters, including etching time, immersion time and immersion concentration have different influences upon wettability, and the best conditions of preparation of superhydrophobic surfaces have been found. The excellent corrosion resistance of the superhydrophobic surface is important for its application in more fields. The outstanding anti-icing and deicing properties of the superhydrophobic surface may be usefully for constructing multifunctional outdoor devices, and may have important potential applications. The non-rigorous conditions are beneficial for the fabrication of large-area surface. This facile and low-cost preparation method is not only favorable for the promising applications of aluminum material for various industrial items, but also offers an effective strategy to fabricate superhydrophobic surfaces on other metallic materials.

Supplementary Information

Video S1: The water droplet sliding on the resulting superhydrophobic surface.

Video S2: Deicing property of the resulting superhydrophobic surface.

Acknowledgments

We gratefully acknowledge the National Natural Science Foundation of China (No. 21271027) for this work.

Notes and references

School of Chemistry, Beijing Institute of Technology, Beijing 100081, P.R. China.
E-mail: shixianglu@bit.edu.cn (S.X. Lu); xuwg60@bit.edu.cn (W.G. Xu)
Fax: +86 10 68912631; Tel: +86 10 68912667

1 W. Barthlott and C. Neinhuis, *Planta*, 1997, **202**, 1.
2 R. Wang, K. Hashimoto, A. Fujishima, M. Chikuni, E. Kojima, A. Kitamura, M. Shimohigoshi and T. Watanabe, *Nature*, 1997, **388**, 431.
3 X.W. Lia, Q.X. Zhang, Z. Guo, T. Shi, J.G. Yu, M.K. Tang and X.J. Huang, *Appl. Surf. Sci.*, 2015, **342**, 76.
4 H. Bellanger, T. Darmanin, E.T. Givenchy and F. Guittard, *Chem. Rev.*, 2014, **114**, 2694.
5 K.S. Liu, M.Y. Cao, A. Fujishima, and L. Jiang, *Chem. Rev.*, 2014, **114**, 10044.
6 L. Zhang, N. Zhao and J. Xu, *J. Adhes. Sci. Technol.*, 2014, **28**, 769.
7 H.C. Barshilia, A. Chaudhary, P. Kumar and N.T. Manikandanath, *Nanomaterials*, 2012, **2**, 65.
8 J. Victor, D. Facchini and U. Erb, *J. Mater. Sci.*, 2012, **47**, 3690.
9 H.S. Lim, J.H. Baek, K. Park, H.S. Shin, J. Kim and J.H. Cho, *Adv. Mater.*, 2010, **22**, 2138.
10 S.H. Park, S.M. Lee, H.S. Lim, J.T. Han, D.R. Lee, H.S. Shin, Y. Jeong, J. Kim and J.H. Cho, *ACS Appl. Mater. Interfaces*, 2010, **2**, 658.
11 S.Y. Gu, Z.M. Wang, J.B. Li and J. Ren, *Macromol. Mater. Eng.*, 2010, **295**, 32.
12 Q.F. Xu, J.N. Wang and K.D. Sanderson, *ACS Nano*, 2010, **4**, 2201.
13 R.V. Lakshmi, T. Bharathidasan and B.J. Basu, *Appl. Surf. Sci.*, 2011, **257**,10421.
14 K. Nakata, S. Nishimoto, A. Kubo, D. Tryk, T. Ochiai, T. Murakami and A. Fujishima, *Chem.-Asian J.*, 2009, **4**, 984.
15 Y. Zhao, Z. Xu, X. Wang and T. Lin, *Langmuir*, 2012, **28**, 6328.
16 Y.H. Kim, Y.M. Lee, J.Y. Lee, M.J. Ko and P.J. Yoo, *ACS Nano*, 2012, **6**, 1082.
17 Q.C. Xu, D.V. Wellia, M.A. Sk, K.H. Lim, J.S.C. Loo, D.W. Liao, R. Amal and T.T.Y. Tan, *J. Photoch. Photobio. A*, 2010, **210**, 181.
18 J. Wang, D. Li, R. Gao, Q. Liu, X. Jing, Y. Wang, Y. He and M. Zhang, *Mater. Chem. Phys.*, 2011, **129**, 154.
19 L. Yin, Y. Wang, J. Ding, Q. Wang and Q. Chen, *Appl. Surf. Sci.*, 2012, **258**, 4063.
20 X.H. Chen, Y.G. Bin, L.H. Kong, D. Dong, L.G. Yu, J.M. Chen and P.Y. Zhang, *Cryst. Growth Des.*, 2009, **9**, 2656.
21 C.R. Crick, J.C. Bear, P. Southern and I.P. Parkin, *J. Mater. Chem. A*, 2013, **1**, 4336.
22 P. Marchand, I.A. Hassan, I.P. Parkin and C.J. Carmalt, *Dalton Trans.*, 2013, **42**, 9406.

23 C.R. Crick and I.P. Parkin, *J. Mater. Chem.*, 2011, **21**, 14712.

24 N. Zhang, S.X. Lu, W.G. Xu and Y. Zhang, *New J. Chem.*, 2014, **38**, 4534.

25 J.X. Wang, S.X. Lu, W.G. Xu and Y. Zhang, *RSC Adv.*, 2014, **4**, 39197.

26 Y.Y. Cheng, S.X. Lu, W.G. Xu and H.D. Wen, *RSC Adv.*, 2015, **5**, 15387.

27 T. Darmanin, E. Taffin de Givenchy, S. Amigoni and F. Guittard, *Adv. Mater*., 2013, **25**, 1378.

28 M. Wolfs, T. Darmanin and F. Guittard, *RSC Adv*., 2013, **3**, 647.

29 H. Bellanger, T. Darmanin, E. Taffin de Givenchy and F. Guittard, *J. Mater. Chem. A*, 2013, **1**, 2896.

30 T. Pauporte, G. Bataille, L. Joulaud and F.J. Vermersch, *J. Phys. Chem. C*, 2010, **114**, 194.

31 H.Y. Gao, S.X. Lu, W.G. Xu, S. Szunerits and R. Boukherroub, *RSC Adv.*, 2015, 5, 40657.

32 F. Guo, X. Su, G. Hou and P. Li, *Colloid Surf. A-Physicochem. Eng. Asp.*, 2012, **401**, 61.

33 X. Xu, Z. Zhang, F. Guo, J. Yang, X. Zhu, X. Zhou and Q. Xue, *Colloid Surf. A-Physicochem. Eng. Asp.*, 2012, **396**, 90.

34 D.Y. Zang, F. Li, X.G. Geng, K.J. Lin and P.S. Clegg, *Eur. Phys. J. E*, 2013, **36**, 59.

35 C.F. Tian, F.L. Zhang, H.H. Cai, J.X. Fang and B.J. Ding, *Mater. Sci. Tech-Lond*., 2013, **29**, 446.

36 X. Qi, W. Song, Z. Mao, W.R. Gao and Q. Cong, *J. Bionic. Eng.*, 2013, **10**, 377.

37 L.J. Liu, J.S. Zhao, Y. Zhang, F. Zhao and Y.B. Zhang, *J. Colloid Interface Sci*., 2011, **358**, 277.

38 N.K. Renukaa, A.V. Shijinaa, A.K. Praveena and C.U. Anizb, *J. Colloid Interface Sci*., 2014, **434**, 195.

39 Y. Wang, W.L. Wang, Y.X. Chen, J.H. Ma and R.F. Li, *Chem. Eng. J.*, 2014, **250**, 248.

40 L.B. Khalfallah, A. Ghorbel, P. Grange and F. Figueras, *Appl Catal B: Environ*, 2005, **59**, 105.

41 L.Y. Gao, D.S. Zhang, Y.J. Wang, W. Xue and X.Q. Zhao, *Reac Kinet Mech Cat*, 2011, **102**, 377.

42 F.T. Lia, Y. Zhao, Q. Wang, X.J. Wang, Y.J. Hao and R.H. Liu, D.S. Zhao, *J. Hazard. Mater.*, 2015, **283**, 371.

43 J.S. Bing, C. Hu, Y.L. Nie, M. Yang, and J.H. Qu, *Environ. Sci. Technol.*, 2015, **49**, 1690.

44 K.W. Yao, S. Jaenicke, J.Y. Lin and K.L. Tan, *App. Catal. B: Environ.*, 1988, **16**, 291.

45 E. Moretti, M. Lenarda, L. Storaro, A. Talon, T. Montanari, G. Busca, E. Rodriguez-Castellon, A. Jimenez-Lopez, M. Turco, G. Bagnasco and R. Frattini, *Appal. Catal. A: Gen.*, 2008, **335**, 46.

46 F.E. Lopez-Suarez, A. Bueno-Lopez and M.J. Illan-Gomez, *Appl. Catal. B: Environ.*, 2008, **84**, 651.

47 http://www.lasurface.com.

48 R.N. Wenzel, *Ind. Eng. Chem.*,1936, **28**, 988.

49 A.B.D. Cassie and S. Baxter, *Trans. Faraday Soc*.,1944, **40**, 546.

50 S.A. Kulinich, M. Farzaneh, *Cold Reg. Sci. Technol.*, 2011, **65**, 60.

51 Q. Jiang and H.M. Lu, *Surf. Sci. Rep.*, 2008, **63**, 427.

52 A. Bondi, *Chem. Rev*., 1953, **52**, 417.

53 X.M. Shi, T.A. Nguyen, Z.Y. Suo, J.L. Wu, J. Gong and R. Avci, *Surface & Coatings Technology*, 2012, **206**, 3700.

54 L. Huang, S.P. Lau, H.Y. Yang, E.S.P. Leong and S.F. Yu, *J. Phys. Chem. B*, 2005, **109**, 7746.

55 X.J. Feng, L. Feng, M.H. Jin, J. Zhai, L. Jiang and D.B. Zhu, *J. Am. Chem. Soc*., 2004, **126**, 62.

56 Y. Liu, X.M. Yin, J.J. Zhang, S.R. Yu, Z.W. Han and L.Q. Ren, *Electrochim. Acta*, 2014, **125**, 395.

57 S.N. Saud, E. Hamzah, T. Abubakar, H.R. Bakhsheshi-Rad, S. Farahany, A. Abdolahi and M.M. Taheri, *J. Alloy Compd*., 2014, **612**, 471.

58 S.A. Kulinich and M. Farzaneh, *Appl. Surf. Sci.*, 2009, **255**, 8153.

59 Y.Y. Wang, J. Xue, Q.J. Wang, Q.M. Chen and J.F. Ding, *ACS Appl. Mater. Interfaces*, 2013, **5**, 3370.

60 Y.D. Yan, N.Z. Luo, X.G. Xiang, Y.M. Xu, Q.H. Zhang and X.L. Zhan, *Prog. Chem.*, 2014, **26**, 214.

61 S.A. Kulinich, S. Farhadi, K. Nose and X.W. Du, *Langmuir*, 2011, **27**, 25.